High Temperature Polymer Electrolyte Membrane Fuel Cell Degradation provoked by Ammonia as Ambient Air Contaminant

Dana Schonvogel[a], Julian Büsselmann[a], Henrike Schmies[a], Hendrik Langnickel[b], Peter Wagner[a], and Alexander Dyck[b]

[a] German Aerospace Center, Institute of Engineering Thermodynamics, Germany

[b] German Aerospace Center, Institute of Networked Energy Systems, Germany

Corresponding author:

Julian Büsselmann

julian.buesselmann@dlr.de

Carl-von-Ossietzky-Str. 15

26129 Oldenburg

Germany

Keywords

High Temperature PEM Fuel Cells

Membrane Electrode Assembly

Durability

Air Pollution

Ammonia

Abstract

High temperature polymer electrolyte membrane fuel cells (HT-PEMFCs) are used from stationary to mobile applications and have the advantage of increased tolerances against fuel impurities like H_2S and CO. However, air impurities can limit their performance and durability. Here, the impact of NH_3-contaminated air is studied during 500 h of operation. 10 ppm NH_3 in air provokes a voltage decay of at least -279.3 µV h^{-1} compared to -18.1 µV h^{-1} during operation without NH_3 demonstrating strong sensitivity of the HT-PEM technology to this air pollutant. Cyclic voltammetry shows a selectively poisoned catalyst, whereby the loss of electrochemical surface area seems to be of no importance. Impedance spectroscopy reveals affected electrode charge transfer processes and strongly affected proton conductivity. µ-computed tomography illustrates significant membrane thinning being significantly larger compared to the blank reference cell. Ion chromatography further indicates that ammonium is incorporated into the cell, so that ammonia is believed to trap the protons stemming from phosphoric acid and hydrogen oxidation reaction. In conclusion, HT-PEMFC degradation caused by ammonia naming formation and incorporation of ammonium species and formation of nitrogen species interacting with the catalyst are identified.

1. Introduction

The PEM fuel cell technology plays a major role in an energy supply based on sustainability. High temperature PEM fuel cells are used in several fields like portable, mobile or stationary applications and are operated at elevated temperatures around 160 °C, which allows a simplified heat and water management and has the advantage of increased catalyst tolerances against fuel contaminants like CO or H_2S.[1-3] Although the HT-PEMFC is characterized by robustness against these fuel contaminants, air contaminants can occur in urban and rural areas and enter fuel cell systems via the cathode gas inlet. Next to sulfur oxides and nitrogen oxides stemming from raw oil-based fuel combustion in vehicle exhausts and industrial plants,[4-5] ammonia is present in ambient air mainly caused by agricultural industry in terms of livestock farming, fertilization and in biogas plants and furthermore by industrial processes and

traffic.[4] The ammonia concentration strongly depends on the environment and location of the fuel cell system. Concentrations can be in ppb-range for urban areas, whereas Wang et al. found peak concentrations up to 279 ppb in Shanghai,[6] and in ppm-range for rural areas, whereas Groot Koerkamp et al. found especially in poultry and pig farms concentrations between 5–30 ppm.[7]

In the past, impacts of air contamination on LT-PEMFCs have comprehensively been investigated.[5, 8-10] Sulfur dioxide leads to cell degradation showing a continuously linear loss of voltage, which is dependent on the extent of contamination and is irreversible. Cell recovery can only be achieved through electro-oxidation of sulfur species, adsorbed on the catalyst, using potential cycling.[11-15] Garsany et al. investigated the oxygen reduction reaction (ORR) of SO_2-poisoned platinum catalysts in an electrochemical half-cell. Adsorbed sulfur species led to significant loss of mass activity and a changed reaction mechanism from 4-electron to the 2-electron pathway.[16-17] On PEM single cell level, they further compared the effect of SO_2 and H_2S on polybenzimidazole (PBI) and perfluorosulfonic acid based membranes and concluded a much larger resistance of PBI against these contaminants.[18] Recently, Reshetenko et al. tested LT-PEMFC poisoning effects and showed reduction and oxidation of SO_2 contaminant at current densities between 0.1–1.0 A cm^{-2}.[19] They further showed the presence of sulfur in oxidation state zero on cathodic platinum below a cell voltage of 0.6 V, which resulted into a dramatic voltage loss.[20] Quijada et al. performed cyclic voltammetry experiments on Pt electrodes during SO_2 contamination and found irreversible changed platinum surfaces.[21-22] On the other hand, the performance of HT-PEMFCs is not significantly affected by SO_2.[15, 23]

Nitrogen monoxide and dioxide also lead to cell degradation of LT-PEMFCs, which depends on several operating parameters and results in slower voltage loss with a constant residual voltage in contrast to SO_2. Cell recovery is achieved by simple prevention of NO_x contamination in the air stream.[12, 15] Chen et al. showed that nitrogen species adsorb on the platinum catalyst surface and decrease the electrochemical surface area (ECSA) without inhibiting the ORR itself.[24] Talke et al. studied the impact of NO_x on single cell and stack level and reported that rather NO than NO_2 is the critical compound for LT-PEMFCs caused by blocking the Pt catalyst surface.[10] In case of HT-PEMFCs, nitrogen oxides also evoke

a strong loss of cell performance. However, a successful recovery of cell performance has not been achieved yet.[15, 25]

Impacts of ammonia on LT-PEMFCs have been studied in terms of air pollution entering the cathode and furthermore in terms of fuel pollution entering the anode. Talke et al. reported the on-going performance loss during LT-PEM single cell and stack operation using an air flow containing 10 ppm ammonia. Indicated by electrochemical impedance spectroscopy (EIS) and cyclic voltammetry (CV) experiments, they found that NH_3 affects several components in LT-PEMFCs. Two processes were assumed to occur simultaneously. Ammonia might chemically react with perfluorosulfonic acid based ionomer and membrane, and ammonia might be electro-oxidized to form nitrogen monoxide which inhibits the catalyst .[10] Zhang et al. reported similar observations on LT-PEMFC contamination with ammonia after EIS and CV experiments.[26] Another study on LT-PEMFCs also reported the impaired proton conductivity of perfluorosulfonic acid based membranes and postulated the simple acid-base reaction increasing the pH and forming NH_4^+, which remains inside the membrane because of less mobility compared to H^+.[27]

Halseid et al. tested the LT-PEM fuel cell using 10 ppm ammonia in hydrogen flow and reported that the hydrogen oxidation reaction (HOR) as well as the ORR were affected.[28] They further investigated NH_4^+ interaction with the Pt catalyst in acidic environments using a three-electrode-setup and detected N_2 and NO during electro-oxidation of NH_4^+ on the platinum surface by differential electrochemical mass spectrometry. Additional stable N- and N-O-species seemed to adsorb and remain on the catalyst surface, so that hydrogen and oxygen reactions and thereby the HOR and ORR were reduced. Thus, these adsorbates were assumed to impede activity and selectivity of the catalyst.[29] Gomez et al. operated the LT-PEMFC exposed to 200 ppm ammonia in fuel stream and found significant impacts on proton conductivity as well as on HOR and ORR, whereas the HOR was affected worst.[30]

Yuan et al. combined LT-PEMFC-testing using a contaminated air flow and catalyst-testing using the rotating disk electrode (RDE) technique. They demonstrated a higher ammonia impact at increased concentration, decreased relative humidity and decreased temperature but independency of the applied current density.[31] Operational temperatures of 40, 60, and 80 °C were considered and resulted into

lower cell degradation at increased temperature. In case of HT-PEMFCs, this study would assume that operation at around 160 °C would cause much less cell damage by ammonia.

On the one hand, studies on HT-PEMFC operation in presence of ammonia contamination are remarkably rare. On the other hand, findings described above related to the LT-PEM technology cannot be adapted completely to HT-PEMFCs because of different cell components and different cell operation parameters. In current literature it is reported that air contamination by NH_3 causes a strong and linear decrease of HT-PEMFC performance dependent on the extent of contamination and that cell recovery by utilizing purified air is not possible.[15] Llerena et al. recently compared HT-PEMFC to LT-PEMFC performances in presence of NH_3-contaminated fuel and showed the recovery of LT-PEMFC by pure hydrogen but irreversible damage of the HT-PEMFC.[32] This points out the importance of understanding electrochemical, physical and chemical degradation processes taking place in HT-PEM based cells being provoked by ammonia. The formation of ammonium phosphate due to reaction with the phosphoric acid electrolyte was discussed but unfortunately not evidenced in this study.[32] In the past, Szymanski et al. tested the phosphoric acid fuel cell (PAFC) tolerance against ammonium in half-cell tests by adding $NH_4H_2PO_4$ to the electrolyte of the cathodic electrode chamber at 191 °C.[33] They found a strong loss of cathode activity of around 84 % after adding 1 wt% of $NH_4H_2PO_4$.

Lee et al. developed and presented a new PEM type using a polyphenylene membrane doped with benzyltrimethylammoniumbiphosphate, which allows operation temperatures between 80–160 °C and showed a stable proton conduction and cell performance.[34] Any cell impairment due to presence of ammonium was not reported. Recently, Cinti et al. presented a design and modeling of a HT-PEMFC system operated with ammonia as storage possibility for green hydrogen and including a reactor for NH_3 decomposition.[35] A total system efficiency of 40 % is achieved, whereby a decomposition temperature above 600 °C is required to ensure complete conversion of NH_3 into H_2. In their experimental studies they considered the presence of N_2 without considering residual NH_3 in the fuel stream. However, because residual amounts of ammonia cannot be excluded, they recommended reducing the ammonia content in the fuel stream by filtering, absorption or adsorption processes.

We recently investigated the platinum contamination by $NH_4H_2PO_4$ using rotating ring disk electrodes and phosphoric acid electrolyte at room temperature and compared the results with the HT-PEM single cell operation for 500 h using 10 ppm of NH_3 contamination in air flow, which present the basis of this study here.[36] Decrease of ORR activity and a changed ORR mechanism from 4-electron to 2-electron pathway by adsorbed nitrogen species was shown and discussed as one reason for the dramatic loss of HT-PEMFC performance.[36] In frame of presenting µ-computed tomography (µ-CT) as visualizing tool for degradation phenomena, we recently showed an increased porosity of bipolar plates caused by presence of SO_2 during HT-PEMFC operation.[37] Furthermore, a changed morphology of membrane electrode assembly (MEA) caused by presence of NH_3 in terms of membrane thinning was shown, which further serves as basis for this study here.[37] However, the detailed understanding of degradation processes inside HT-PEMFCs provoked by ammonia has not been given yet. This study brings our first results[36-37] together with a comprehensive investigation by use of electrochemical methods during HT-PEM single cell operation including polarization curves, EIS and CV and by use of further analytical methods to analyze single components after operation. This includes imaging of MEA and catalyst particles by µ-CT and transmission electron microscopy (TEM) as well as product water analysis by ion chromatography (IC) and pH value measurements. Following questions are addressed in this study: What are the electrochemical, chemical and physical processes during HT-PEMFC operation which are influenced by or arise from ammonia? And what are the consequences for the HT-PEM fuel cell type and its stability?

2. Experimental

2.1 Membrane Electrode Assembly

MEAs were purchased from Advent Technologies SA (Greece) and were APM-25 types with an active area of 20.25 cm^2, which are similar to the Celtec® P1100W technology licensed by BASF SE (Germany). Thus, the electrolyte membrane consists of PBI doped with phosphoric acid. The cathode catalyst consists of platinum-nickel alloy nanoparticles deposited on Vulcan® XC-72R and the anode catalyst consists of platinum nanoparticles deposited on Vulcan® XC-72R. Woven gas diffusion layers (GDL) with microporous layer are used on both sides. Deeper information of MEA assembly, acid doping level and catalyst loadings are confidentially given by the manufacturer and cannot be disclosed. In the following performed experiments, all tested MEAs stem from the same manufacturing batch. In consequence, the maximum comparability of the MEAs is guaranteed, so that impacts of NH_3 are revealed.

2.2 Fuel Cell Test Procedure

For all experiments, a test station from inhouse engineering GmbH (Germany) was used, which is constructed for PEM single cells and equipped with a cell compression unit from balticFuelCells GmbH (Germany). The cell contains bipolar plates (BPP) of graphite with polyphenylene sulfide purchased from Eisenhuth GmbH & Co. KG (Germany), designed for HT-PEM fuel cells.

MEAs were fixed between the BPPs inside the cell by the compression unit. The cell was flushed with nitrogen through cathode and anode gas inlets and heated up to 120 °C. Then, the reactant gases hydrogen and air were supplied followed by applying a load current density of 0.3 A cm^{-2} and further heating up to the final temperature of 160 °C. Before cell characterization at begin of test (BoT) described later, the break-in was carried out for 48 h using the operational parameters in Table 1. After BoT characterization, the cells were operated for 500 h using same operational parameters. When the cells reached the operating duration of 500 h, a second cell characterization at the end of test (EoT) was performed and is described later in more detail.

Four MEAs from the same manufacturing batch were operated in this way. Two MEAs were fed with dry air containing 10 ppm ammonia, which is in the following called "NH_3 test". And two further MEAs were fed with uncontaminated dry air called "blank test".[36] The NH_3 concentration of 10 ppm was ensured by mixing oxygen and compressed air with nitrogen containing 20 ppm ammonia, which was automatically controlled by the test station. Choosing this mixture avoided any interruption of the gas supply during the tests.

Table 1 Operation parameters during the four MEA tests.

Temperature / °C	160
Current density / A cm^{-2}	0.3
Operation time / h	500
Reaction gases (stoichiometry) of anode and cathode	Dry hydrogen (1.5) and dry air (2.0)
Gas pressure / atm	1
Contact pressure between MEA and BPP / MPa	0.75

2.3 Electrochemical Characterization

Each cell was characterized twice (BoT and EoT) by performing the following electrochemical methods. Thereby, measurements in BoT stage were more extensive than in EoT stage, because after operation in the presence of NH_3 it was important to maintain the MEA properties after contamination. Provoking larger changes in the MEAs by applying extensive electrochemical measurements at EoT was avoided, because the MEAs were removed from the test station afterwards and underwent further physical analyses to identify contamination effects.

In BoT stage, a polarization curve was recorded first by controlled changing of current densities. The current density started at 0.3 A cm^{-2} and was increased to 1.0 A cm^{-2} using current steps of 0.5 A for 30 s.

Then, decrease until reaching open circuit voltage (OCV) followed by a second increase up to 1.0 A cm^{-2} and a second decrease back to 0.3 A cm^{-2} was applied. The second current increase stage was used for data evaluation within each MEA testing. Second, EIS measurements were carried out at current densities of 0.03, 0.1, 0.2, 0.3 and 0.4 A cm^{-2} after connecting the potentiostat Modulab 2100A and external booster 12V/20A from Solartron Analytical (United Kingdom) to the cell. For each current density an AC perturbation amplitude of 10 mV (rms) in a range of frequencies between 100 kHz–100 mHz using a logarithmic distribution was applied and resulting in ten steps per decade and one additional step at 100 mHz. Additional to the BoT stage, EIS was further performed at 0.3 A cm^{-2} after 72, 260 and 430 h of cell operation to monitor changes in the cell resistance during the test period. To analyze the degradation processes the impedance spectra were fitted with the equivalent circuit of Figure 1. Detailed descriptions about this equivalent circuit modelling are provided in previous studies.[38-39] The software RAVDAV was used for fitting of the spectra.[40]

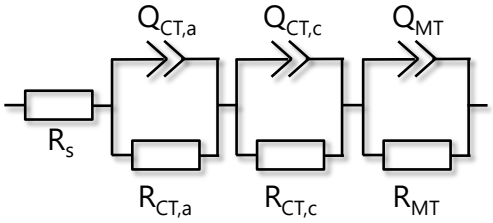

R_s: Serial Resistance
$R_{CT,a}Q_{CT,a}$: Charge Transfer Anode
$R_{CT,c}Q_{CT,c}$: Charge Transfer Cathode
$R_{MT}Q_{MT}$: Mass Transport

Figure 1 Scheme of the equivalent circuit for the fitting of impedance spectra, which contains a serial resistance (R_s) followed by three RQ-elements. More descriptions are given in literature.[38-39]

Third, the potentiostat Modulab 2100A from Solartron Analytical (United Kingdom) was connected to the cell to carry out the following voltammetry measurements. The cathode was considered as working electrode and the anode was considered as reference and counter electrode. Thereby, first the test station integrated electrical load was switched off. The cathode gas was changed to nitrogen with a flow rate of 100 mL min^{-1} and the anode gas was set to hydrogen with a flow rate of 100 mL min^{-1}. CV curves were recorded at a cell temperature of 160 °C and a scan rate of 100 mV s^{-1} in the potential range of

0.05–1.0 V_{RHE} by applying seven cycles. In case of linear sweep voltammetry (LSV) gas flow rates of 300 mL min^{-1}, a potential window of 0.19–0.50 V_{RHE} and a scan rate of 2 mV s^{-1} were used. The LSV data were applied for CV curve correction considering the internal shortcut current. The CV data were applied to calculate the ECSA.

In EoT stage, the numbers of measurements were shortened to treat the MEAs carefully after cell operation of 500 h. Thus, the current densities counting 0.03, 0.1, 0.2, 0.3 and 0.4 A cm^{-2} were used to perform EIS measurements on the one hand and were further used to generate a quasi-polarization curve on the other hand. Voltammetry experiments were identical to the experiments in BoT stage.

2.4 Physical Characterization

µ-computed tomography for visualization of the tested MEAs and its components was performed on a desktop µ-CT SkyScan 1172 (Bruker MicroCT, Belgium). Samples with a diameter of 6 mm were punched from the center area of the tested MEAs and placed horizontally on a metallic sample holder. Two samples of each MEA were measured. Table 2 lists the parameters of the µ-CT measurement and the following reconstruction process which was performed using the NRecon software (Bruker MicroCT, Belgium). In this step, grey scales of the measurements were kept the same to ensure comparability for the visualized images. After the reconstruction, a defined volume of interested (VOI) with dimension of 700x700x400 pixels was selected using the software DataViewer. In a next step, the images were obtained from the software CTVox.

Layer thickness of cathode, membrane and anode were defined in the program DataViewer. Of each measured MEA, two cross sectional areas were chosen and the thickness of each individual layer was measured at 20 different positions. Mean values and standard deviations were calculated from analyzing in total four cross sections per MEA.

Table 2 Overview of chosen parameters of the µ-CT measurement and reconstruction.

Parameter / Unit	Value
Acceleration Voltage / kV	78-82
Current / µA	96-104
Rotation Step / °	0.2
Random Movement	4
Averaging Frames	10
Resolution / µm pxl^{-1}	1.7-2.1
Exposure Time / ms	1350
Stage temperature / °C	22.0-25.2
Reconstruction Grey Scale	0-0.11

Product water vapors were continuously condensed and collected directly after cathodic and anodic gas outlets of the single cell, taken in defined periods (after break-in, after BoT and then every week) and analyzed by ion chromatography (IC) using the 850 Professional IC from Metrohm AG (Switzerland). To control a possible formation of nitrogen containing ions during HT-PEMFC operation followed by removal from the cell by the water phase, nitrate and ammonium concentrations of the collected waters were monitored over time of cell operation and quantified with stock solutions (1000 mg L^{-1} in water, TraceCERT® from Fluka, Sigma Aldrich Corporation, United States or Merck KGaA, Germany). Control measurements were carried out by the TraceCERT® Multi Anion Standard 1. Water pH values were measured by the ProLab4000 pH meter from Schott Instruments GmbH (Germany). In an additional experiment, one MEA was further investigated by IC after the NH_3 test. To examine the existence of ammonium phosphate inside the MEA and its deposition during cell operation, three similar pieces of the MEA after

cell operation (area of 0.5 cm^2) were punched out and stirred in 30 mL of deionized water at 50 °C for 50 h. The aqueous solution was then analyzed on ammonium by IC.

Furthermore, the MEA was investigated after immediate removal from the HT-PEMFC test bench by analyzing the catalyst using transmission electron microscopy (TEM). Therefore, the cathode layer was separated from the other layers using a scalpel and dispersed in ethanol via ultra-sonication. The suspensions were then dropped on 200 mesh copper grids coated with polyvinylformal from Plano GmbH (Germany). After atmospheric drying, the grids were transferred into the EM 902A from Carl Zeiss AG (Germany) equipped with tungsten cathode and CCD camera. Images were displayed at an acceleration voltage of 80 kV and afterwards evaluated on the Pt particle diameter on basis of averaging 300 diameters using the ImageJ software.

3. Results and Discussion

3.1 Electrochemical Results

In the following, the electrochemical investigations of contaminated and un-contaminated HT-PEM single cells during 500 h of operation are compared and discussed. Voltages over time of operation are shown in Figure 2a) in case of NH_3 testing compared to blank testing with repeating measurements each. The NH_3 tested cells show different starting voltages in BoT stage of 0.64 V and 0.62 V, whereas the blank cells show 0.63 V in both cases. These negligible differences in the beginning cell performance point to minimal differences in MEAs caused by manufacturing, because test procedure and test station are identical. Other studies on HT-PEMFC performance dependent on the manufacturing company and reproducibility inside manufacturing batches of MEAs demonstrated the occurrence of inner-batch deviations in cell performance.[41-42]

Blank testing demonstrates a very stable cell voltage over time with high reproducibility. The voltage decay is -12.2 µV h^{-1} and -18.1 µV h^{-1} for the second measurement. In contrast, NH_3 testing causes a large voltage drop within both measurements. Whereas both blank cells show a constant and comparable voltage over time, both NH_3 tested cells prove a highly comparable behavior demonstrating a distinct

linear and continuously ongoing voltage loss over time without reaching any voltage plateau. This means that NH_3 poisoning of HT-PEMFCs is an ongoing and accumulating process without reaching a steady state, which indicates a failure and dying of the cell with the time. The voltage decay is found to be -279.3 µV h^{-1} and -317.2 µV h^{-1} for the second measurement, so that the averaged performance loss is approximately 20 times higher in presence of NH_3 than the loss in absence of NH_3.

Llerena et al. tested HT-PEMFCs adding 50, 150, 300 and 500 ppm of NH_3 into the hydrogen flow for 120 min at a constant voltage of 0.5 V.[32] Whereas applying 50 ppm NH_3 resulted into a current loss of 1 %, changing to higher concentrations led to distinct linear current loss over time. This shows that ammonia poisoning of HT-PEMFCs is not only time-dependent but also concentration-dependent.

Next to studies on cell contamination, other studies on HT-PEMFC degradation investigated impacts of operational conditions instead of poisoning. Yu et al. operated single cells for 500 h applying a load cycling profile including 0.2 and 0.6 A cm^{-2} for 30 min each and open circuit voltage (OCV) for 2 min and found voltage loss rates of -27.9, -41.3 and -34.1 µV h^{-1}.[43] Galbiati et al. tested single cells at 0.2 A cm^{-2} and 160 °C and reported an increased loss rate from -8 to -19 µV h^{-1} by raising the temperature to 180 °C and a decreased loss rate from -8 to -4 µV h^{-1} by doubling the current density to 0.4 A cm^{-2}.[44] Recently, Søndergaard et al. developed a novel cross-linked PBI membrane processed into a HT-PEMFC single cell and presented a very low voltage loss rate of -1.4 µV h^{-1} after 13,000 h.[45] These different studies reported much lower voltage decays compared to this study. The comparison of our degradation study on ammonia contamination with these other studies on impacts of cell operational parameters points out, that the voltage loss rate provoked by ammonia poisoning is much higher than voltage loss rates from literature provoked by applying various operational conditions.

Figure 2b) compares the polarization curves of both blank tests and both NH_3 tests on one hand and the curves before and after 500 h of operation (BoT and EoT) in each case on the other hand. Whereas BoT curves show maximum current densities of around 1.0 A cm^{-2}, the EoT curves are shortened to applied current densities of 0.03, 0.1, 0.2, 0.3 and 0.4 A cm^{-2} in order to avoid additional electrochemical stress after operation. In BoT stage, the curves show small deviations traced back to impacts of MEA

fabrication, which have also been visible by slight different starting voltages in Figure 2a). In contrast, highly deviating curves become visible in EoT stage. Whereas both blank curves at EoT are still comparable to BoT curves, the NH_3 curves are down-shifted to much lower voltages and indicate that next to ohmic range also the activation range is affected by ammonia. The further electrochemical results provide insight into the cell degradation.

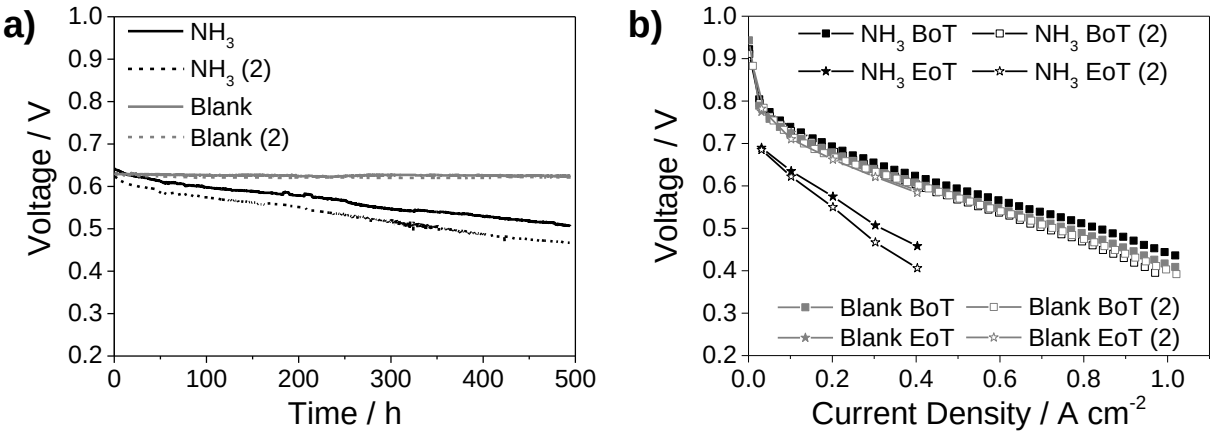

Figure 2 (a) Voltage curves over time of operation and (b) polarization curves before and after cell operation with air contamination – first test "NH_3" (raw data shown in [36]) and repeated test "NH_3 (2)" – and without air contamination – first test "Blank" (raw data shown in [23, 36]) and repeated test "Blank (2)".

At the beginning CV curves were recorded without cell contamination and after 500 h of cell contamination to investigate the degradation of the cathode catalyst. Figure 3a) shows changed curves after NH_3 testing and also after blank testing in all cases. Changes are visible in the range of hydrogen underpotential deposition (HUPD) between approx. 0.0–0.3 V_{RHE}, which can be provoked by the cell operation itself.[46-47] Decreased current densities point to a lowered electrochemically assessable Pt catalyst surface after all tests. However, the exposure to NH_3 leads to differences in the curve shape compared to the blank operation in different potential ranges. These potential ranges are enlarged and displayed in Figure 3b-d).

Figure 3b) illustrates the differences in peak shape of desorption of hydrogen on the platinum surface, whereby exclusively the EoT curves are shown to better illustrate the differences between NH_3 and blank. Both curves after blank operation still possess two overlapping peaks with similar intensities at approx.

0.10 and 0.16 V, respectively, which is assigned to hydrogen oxidation taking place on different Pt facets. This is known for typical spherically shaped Pt nanoparticles on carbon blacks like Vulcan® fabricated in these MEA[48-49] and has also been present in all four BoT curves in Figure 3a). However, both curves after NH_3 operation consist of different peak shapes, which are also enlarged in Figure 3b). They are comparable among each other and show a suppressed peak at approx. 0.10 V and a larger presence of the peak at approx. 0.16 V. This reveals a changed hydrogen sorption behavior on platinum with indication of a selectively poisoned catalyst surface provoked by ammonia.

The next enlarged potential ranges are depicted in Figure 3c-d) and visualize changed oxidation and reduction processes in presence of NH_3, respectively. Figure 3c) shows the range of typical hydroquinone oxidation at around 0.6 V and platinum oxidation starting at a potential greater than 0.6 V.[50-51] BoT curve shapes are comparable in this range, whereby the BoT curve of the first blank operation shows slightly higher currents in the Pt oxidation range. After 500 h of operation with and without ammonia contamination the EoT curves significantly deviate from each other. Blank operation leads to steadily present hydroquinone oxidation at around 0.6 V and an unchanged Pt oxidation range starting at around 0.6 V. In contrast, NH_3 operation leads to suppressed hydroquinone oxidation but highly increased currents in the Pt oxidation range with an indicated peak maximum at approx. 0.8 V. Possible reasons for suppressed hydroquinone oxidation could be a changed carbon surface due to removed oxygen functionalities or rather an impact of ammonia in terms of adsorbed nitrogen species on the carbon. Increased currents in the Pt oxidation range can be caused by additional oxidation reactions caused by ammonia presence. Figure 3d) shows the range of typical quinone reduction at around 0.5–0.6 V. Blank operations show lowered currents after 500 h, while NH_3 operations show distinct increased currents after 500 h. In case of blank operation this points to changed carbon properties in terms of electrode capacity and surface functionalities provoked by the operational conditions themselves. In case of NH_3 operation significantly increased currents might point to additional reduction reactions caused by ammonia presence.

Zhang et al. recorded CV curves at LT-PEMFC cathodes in presence of ammonia and observed slightly reduced peaks in the hydrogen and in the oxygen region but no additionally arising peaks or partially suppressed HUPD and hydroquinone oxidation as found in this study.[26] Contrary to that study, an arisen oxidation peak located at 0.8 V was also found by Halseid et al.[29] They performed CV using ammonium ions in acidic electrolytes to see effects on platinum. In a three-electrode-setup they detected an additional oxidation peak in CV curves at around 0.80 V_{RHE} and an additional reduction peak at around 0.66 V_{RHE} attributed to N- or N-O-species. This observation is similar to results of our study in Figure 3c-d). Electro-oxidation of NH_3 forming nitrogen monoxides was also suggested by Talke et al. after LT-PEM single cell and stack operation.[10]

Possible reactions taking place in our study on the HT-PEM type are listed in the following. First, ammonia adsorbs on the platinum surface according to Equation [1] followed by electrochemical oxidation according to Equation [2]. This is assumed to take place already in the low potential range and might cause the partially blocked Pt surface sites in the HUPD region revealed in Figure 3b). Because the voltage during HT-PEMFC operation here depicted in Figure 2a) is between 0.45–0.65 V, these reactions are presumed to be present and dominate the catalyst degradation. During CV in Figure 3a) a larger potential range is scanned and considered. Further electrochemical oxidation according to Equation [3] can take place at around 0.8 V, where comparably higher currents with an indicated peak maximum have been recorded. A requirement for this reaction is the presence of Pt oxides, which is given at 0.8 V.

Finally, this CV experiment demonstrates the high stability of these nitrogen adsorbates in the applied potential window, so that cell recovery through removal of catalyst poisoning species is obviously not possible in this way.

$NH_{3,g} \rightleftharpoons NH_{3,ads}$ [1]

$NH_{3,ads} \rightleftharpoons N_{ads} + 3e^- + 3H^+$ [2]

$N_{ads} + O_{ads} \rightleftharpoons NO_{ads} + 2e^-$ [3]

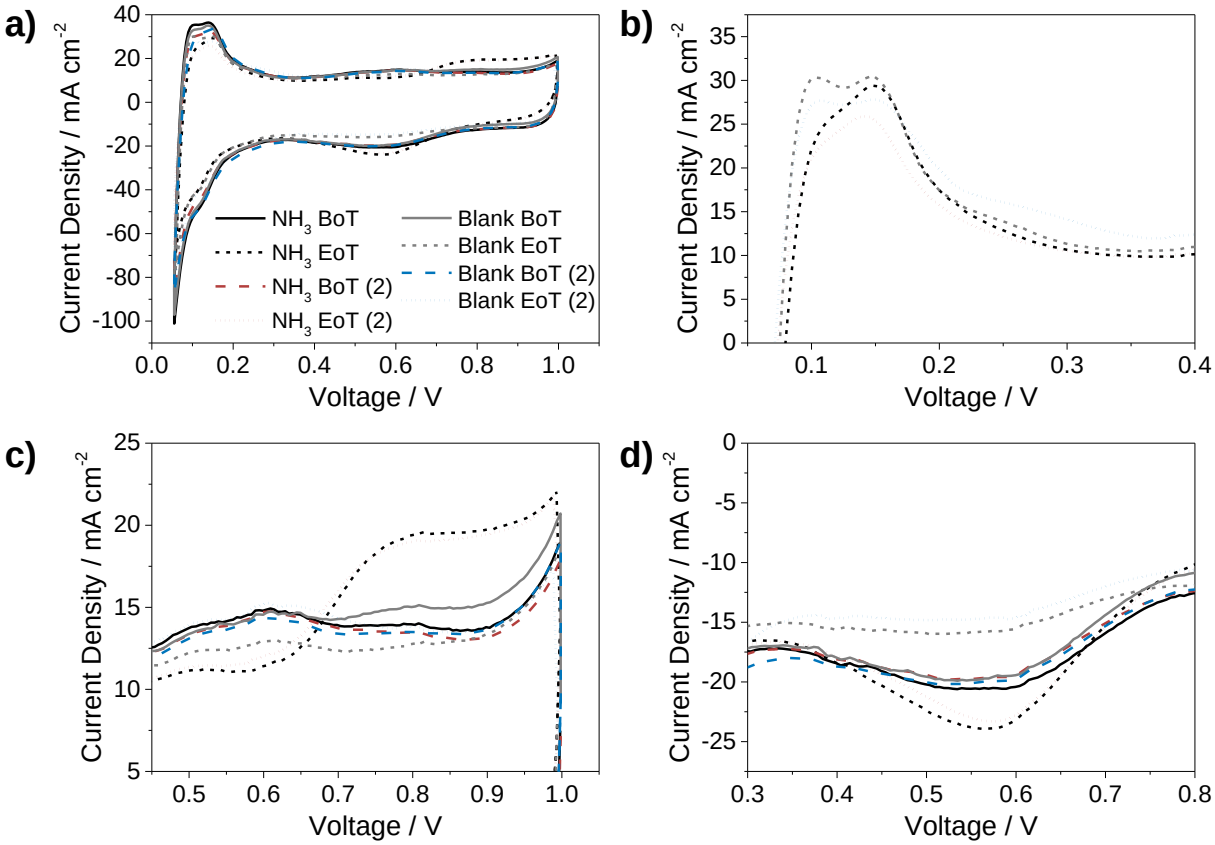

Figure 3 Cyclic voltammetry at a cell temperature of 160 °C before (BoT) and after cell operation (EoT) with air contamination – first test "NH_3" and repeated test "NH_3 (2)" – and without air contamination – first test "Blank" and repeated test "Blank (2)".

The ECSAs are calculated on the basis of HUPD in Figure 3 and Equation [4]. Thereby, hydrogen is electrochemically adsorbed on the surface of the Pt catalyst and is then oxidized during the anodic scan. The resulting CV signal between around 0.0–0.3 V is considered in Equation [4] towards its charge amount Q_{Pt},[44, 52-53] which is then divided by the scan rate ν, the charge density ρ (2.1 C m_{Pt}^{-2}) and the mass of Pt catalyst L_{Pt}. ECSA changed from 11 m^2 g_{Pt}^{-1} to 8 m^2 g_{Pt}^{-1} (-25 %) and from 9 m^2 g_{Pt}^{-1} to 7 m^2 g_{Pt}^{-1} for repeated measurement (-21 %) in case of NH_3 testing and changed from 11 m^2 g_{Pt}^{-1} to 9 m^2 g_{Pt}^{-1} (-21 %) and from 10 m^2 g_{Pt}^{-1} to 8 m^2 g_{Pt}^{-1} for repeated measurement (-22 %) in case of blank testing. Thus, the loss of electrochemical surface area is very comparable. Only slightly larger losses are indicated in presence of ammonia.

ECSA loss can generally originate from catalyst degradation in presence of operational fuel cell conditions, which are identical for all tests. Well-known aging paths of Pt nanoparticles on carbon supports are agglomeration due to Ostwald-Ripening, detachment from support surface or the migration followed by coalescence.[46-47, 54-55] Bandlamudi et al. stressed Celtec®-based MEAs through applying potential switching (0.5/0.9 V, ~5,000 cycles) and thereby provoked ECSA losses greater than 60 %.[56] Galbiati et al. reported for Celtec®-based cells after 6,000 h at 0.2 A cm^{-2} the decrease of ECSA by 59 %.[44] Comparison with other works from the literature on HT-PEMFC degradation reveals, that choice of operation condition is more critical for catalyst aging than an ammonia contaminated air flow. This is contrary to the losses in cell performance discussed on the basis of Figure 2. Performance losses are highly accelerated caused by ammonia in comparison to other works testing several operation conditions. In consequence, other degradation processes despite catalyst poisoning must be much more dominant during ammonia contamination of HT-PEM fuel cells, which is investigated and discussed in the following.

$$ECSA = \frac{Q_{Pt}}{\vartheta \cdot \rho \cdot L_{Pt}} \qquad [4]$$

Figure 4a-b) depicts the Nyquist diagrams of electrochemical impedance spectroscopy recorded in defined periods of operation time. The polarization resistance (R_p) has not significantly changed during blank operation pointing to a very stable cell operation in this case, whereas the NH_3 testing leads to a highly increased polarization resistance. The polarization curves in Figure 2b) have already clarified the stable cell performance during blank operation, whereby ammonia has been indicated to affect the ohmic range as well as the activation range. This is verified here by the impedance results in Figure 4a). The serial resistance (R_s) changed by 9 % from 0.113 to 0.124 Ω cm^2, while the blank operation shows a constant resistance with a change lower than 1 %. The proton conductivity of the electrolyte membrane is thus affected by ammonia, whereas membrane conductivity in case of blank testing remains constant and is unaffected.

Single cell resistances are calculated from impedance fitting using the equivalent electric circuit in Figure 1 and are shown as function of cell operation time in Figure 4c-d). These resistances are very comparable for both tests in BoT stage (time = 0 h), since air contamination has not been applied in this stage. After introducing NH_3 contamination the charge transfer resistance during ORR at the cathode ($R_{CT,c}$) and the mass transport resistance (R_{MT}) become significantly larger, whereas the charge transfer resistance during HOR at the anode ($R_{CT,a}$) shows negligible changes. This demonstrates the inhibited catalyst activity restricted to cathode site, so that hydrogen oxidation and the formation of protons at the anode take place without hindrance. The negative impact of ammonia and ammonia originated species is obviously restricted to the cathode and the electrolyte membrane. The possible diffusion of ammonium ions in perfluorosulfonic acid based membranes was demonstrated in another study.[57] The comparison with CV results in Figure 3 makes clear that nitrogen species interact with the cathode catalyst, which can affect the ORR kinetics. Additionally, ammonia can trap protons at the cathode, so that the ORR mechanism is further affected. EIS studies on the LT-PEM types of Zhang et al.[26] and Gomez et al.[30] also resulted into affected membrane and electrode kinetics.

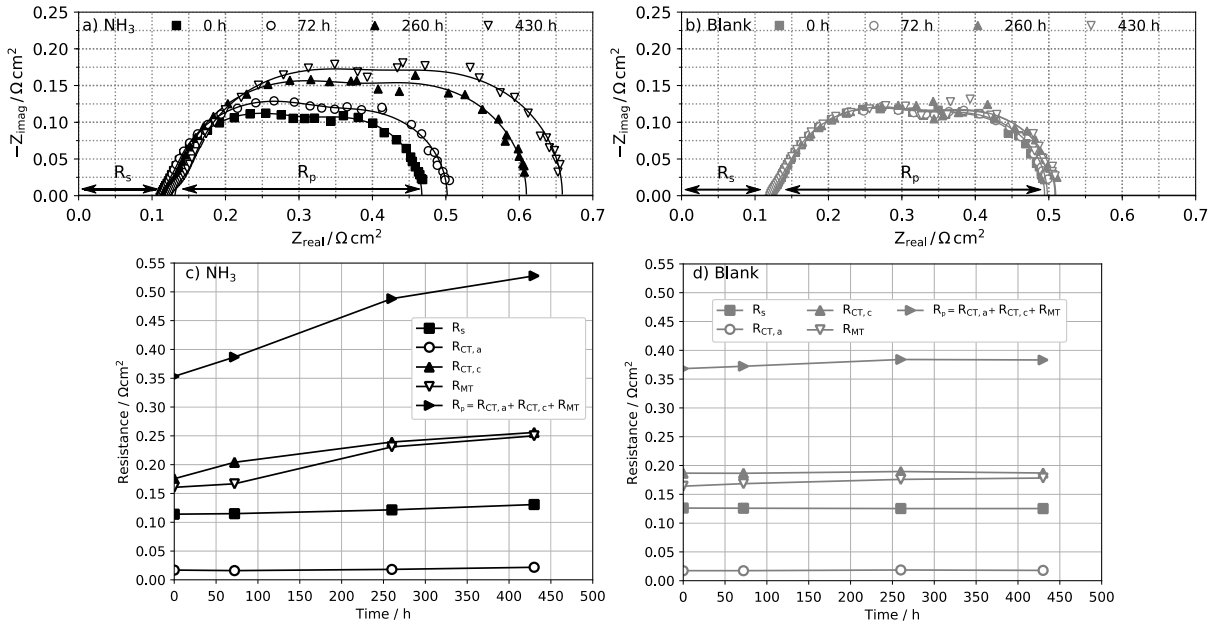

Figure 4 (a) Nyquist diagrams from electrochemical impedance spectroscopy at 0.3 A cm^{-2} during cell operation and corresponding impedance fits (lines, compare Figure 1) with presence of "NH_3" contamination (raw data shown in [36]), (b) Nyquist diagrams without contamination "blank" (raw data shown in [23, 36]), (c) single resistances over time of cell operation determined by the impedance fits with presence of "NH_3" contamination and (d) single resistances without contamination "Blank".

3.2 Physical Results

Figure 5 compares the µ-CT images after cell operations. In order to ensure the additional comparison with the BoT stage of MEAs, one fresh untested MEA of the same manufacturing batch was analyzed in the same way. This MEA is called "pristine" and is shown in Figure 5e). While the pristine MEA consists of very defined and separated layers namely membrane, catalyst layers and gas diffusion layers, the MEAs after NH_3 testing in Figure 5a-b) consist of less defined layers. In particular, interfaces between membrane and catalyst layers are highly indistinct. The arrows illustrate parts of strong layer thinning and delamination. In contrast, the MEAs after blank testing in Figure 5c-d) consist of more distinct interfaces between membrane and catalyst layers, but they also possess less defined and partially thinned layers than the pristine MEA. Such severely affected parts are marked with arrows.

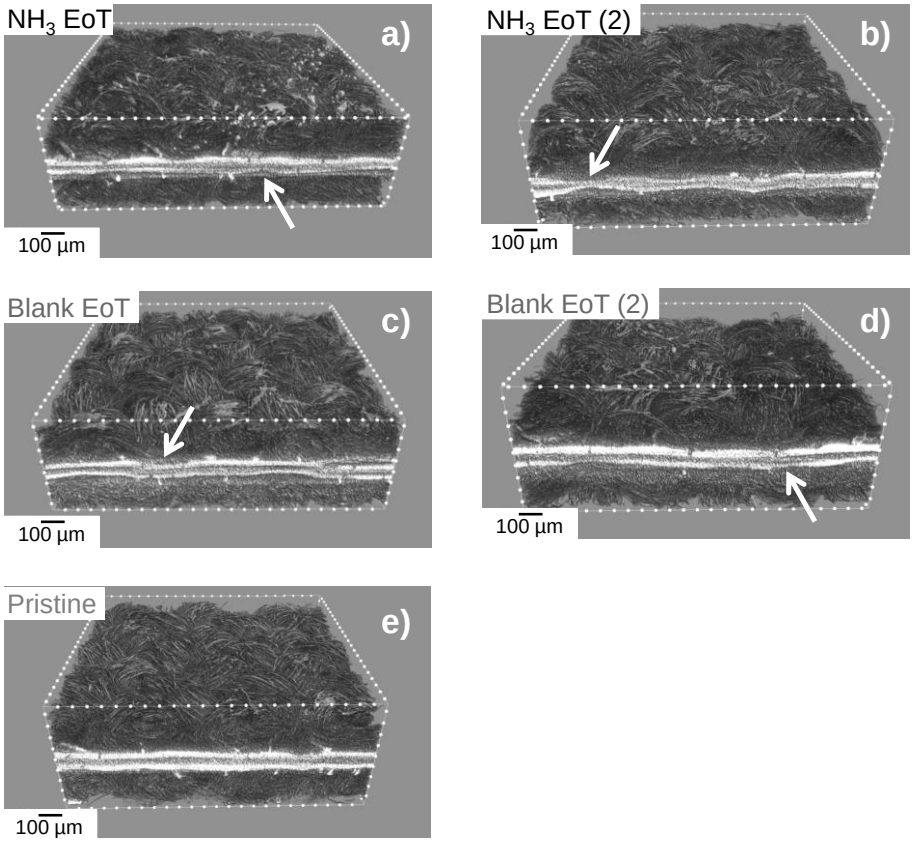

Figure 5 Reconstructed µ-computed tomography images of cross-sectional MEAs showing the cathode on the top (raw data shown in [37]).

Figure 6 shows the layer thicknesses of cathode, membrane and the anode measured from the µ-CT images of the NH_3 tested MEAs and the blank tested MEAs in comparison to the pristine MEA stemming from same manufacturing batch. It is shown that in pristine stage the membrane thickness is 72.8±0.5 µm and the electrode thicknesses are 51.3±2.1 µm for the cathode and 46.5±2.0 µm for the anode. While the cathode thicknesses after each cell operation are not significantly changed, anode thicknesses slightly decreased between 5.1–7.5 µm. Deviating trends in anode and cathode thickness changes depending on cell operation with air contamination and without air contamination are not observed.

This is different in case of the membrane thickness. While the membrane is thinned out by 8 µm or 11 % after the blank operation compared to pristine stage, NH_3 operation provoked much larger membrane thinning by 15 µm or 21 % and 18 µm or 25 %. Also other HT-PEMFC operations led to membrane thinning caused by creeping and further instability aspects due to cell operation implying compression,

heating and generating electricity as known from literature. [58-60] However, the strengthened membrane thinning compared to blank operation in this study is evidenced to be caused by exposing the HT-PEMFC to ammonia itself. Impedance data in Figure 4 showed an increased ohmic resistance and thus decrease of proton conductivity. Membrane thinning would rather lead to decreased ohmic resistances. Thus, another contrary effect dominates the change of proton conductivity in a negative direction.

Proton conduction can be affected by chemical reaction of ammonia with phosphoric acid or with imidazole groups of the PBI polymer. Possible reactions are listed in the following. The acid-base reaction according to Brønsted in Equation [5] for the formation of ammonium cations can take place due to the acidic environment in HT-PEM fuel cells. Next to direct reaction with protons ammonia can deprotonate the phosphoric acid according to Equation [6]. Both possible equilibrium reactions of Equations [5-6] follow the principle of Le Chatelier. This means that both reactions might be shifted to the right side in the beginning of the test because of acid excess and that both reactions might also be shifted to the right side during further operation, because ammonia continuously enters the cell via the air flow. Therefore, ammonia can be present in excess relatively to phosphoric acid during longer cell operation. Next to free phosphoric acid molecules a part of the acid molecules reacts with imidazole groups of PBI. However, this proton donation by H_3PO_4 can be disabled by ammonia, too.

In further consequence, NH_3 entering the cathode can directly trap the protons, which are previously generated at the anode and diffused through the membrane. Lowered presence of protons at the cathodic three-phase-boundary has then an immediate impact on ORR. In overall consequence, presence of NH_3 can hinder the proton conduction not only in the electrodes but also in the membrane leading to an overall loss of HT-PEMFC performance. Although these possible reactions can explain the loss of proton conductivity and the decrease of electrode charge transfers, the direct explanation of observed strong membrane thinning cannot be given. However, precipitation of ammonium phosphate salts and thus ionic bonding of previously free phosphoric acid molecules might consequence a reduced volume and further leads to the observed membrane thinning.

$$NH_3 + H^+ \rightleftharpoons NH_4^+ \quad [5]$$

$$NH_3 + H_3PO_4 \rightleftharpoons NH_4^+ + H_2PO_4^- + NH_3 \rightleftharpoons 2NH_4^+ + HPO_4^{2-} + NH_3 \rightleftharpoons 3NH_4^+ + PO_4^{3-} \quad [6]$$

Llerena et al. reported significant HT-PEMFC performance loss after operation with NH_3-contaminated fuel and discussed the system to be affected by increased activation losses and ohmic losses, which was visible during recording polarization curves.[32] Therefore, they discussed the diffusion of ammonia into the anode, into the phosphoric acid doped membrane and further into the cathode followed by chemical reaction of ammonia with the acid. Scanning electron microscopic imaging of the membrane near to the cathodic layer was presented to discuss the formation of ammonium phosphates. However, the presence of ammonium salts was not evidenced in that study. Here, ion chromatography experiments were carried out to detect ammonium in the product waters and are discussed in the following.

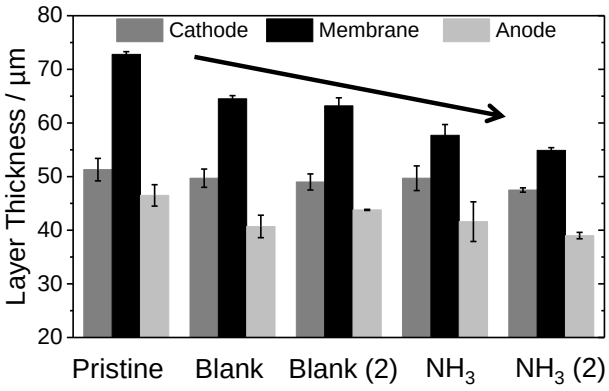

Figure 6 Thicknesses of cathode, membrane and anode of MEAs calculated by the cross-sectional µ-CT images.

Product water vapor was condensed and collected after break-in, after BoT measurements and furthermore every week. Waters were analyzed on containing ions by IC measurements and on their pH value. Figure 7 shows on the one hand nitrate contents and on the other hand ammonium contents to control electrochemical conversion forming NO_3^- or simple acid-base reaction of Brønsted forming NH_4^+ followed by discharge from the cell via the water vapor phase.

Figure 7a-b) compares the nitrate concentrations in cathodic and anodic waters during the two blank and NH_3 operations, respectively. The results show neither decreasing nor increasing trends over time of operation in all cases. The concentrations are mostly below 1 mg L^{-1} near the detection limit and are

in the same range for blank and NH_3 tests. Thus, it is verified that electro-oxidation of NH_3 forming and discharging NO_3^- is not a predominant process taking place during NH_3-contaminated HT-PEMFC operation. In contrast, in another study we showed the electro-oxidation of SO_2 inside the HT-PEMFC and the discharge of SO_4^{2-} via the product water.[23]

Figure 7c) reveals that NH_4^+ concentrations of the cathodic waters are (except two outliers during the first blank test) in range of the detection limit in all cases. Although ammonia gas enters the cathode, ammonium ions do not leave the cathode in detectable amounts. Figure 7d) shows NH_4^+ concentrations of the anodic waters. Whereas most of the waters contain negligible NH_4^+ amounts in range of the detection limit comparable to the cathodic waters, the second NH_3 test results into NH_4^+ concentrations above the detection limit but below 1 mg L^{-1}. While during break-in and BoT measurements the cell was not contaminated by 10 ppm ammonia through the air flow and no ammonium was detected, the operation with ammonia starting in week one then leads to detectable ammonium amounts/concentrations. From week to week this NH_4^+ concentration steadily decreases, although the cell was operated with constant 10 ppm NH_3 in the air flow. This indicates NH_4^+ incorporation into the MEA. However, this trend cannot be verified by the other NH_3 testing in this study. Overall, these results clarify that NH_4^+ is not discharged by anodic or cathodic waters in significant amounts and that NH_3 originating species rather stay and are incorporated inside the MEA. To underline this fact, we estimated the detected amount of NH_4^+ below 0.01 ‰ of the applied NH_3 amount during 500 h.

The assumption of NH_4^+ incorporation into the MEA is plausible since the ammonium phosphate salts in Equation [6] are namely water soluble, however, in presence of HT-PEMFC conditions the produced water is in vapor phase. To proof the presence of water soluble and incorporated ammonium salts, a sample of the contaminated MEA after first NH_3 testing was stirred in heated water to dissolve such ammonium salts. Stirring of the MEA samples (three pieces with areas of 0.5 cm^2) in 30 mL H_2O at 50 °C for 50 h indeed leached out ammonium. The measured NH_4^+ concentration is 7.53±1.46 mg L^{-1}, which corresponds to 0.6 ‰ of the applied NH_3 amount after 500 h of operation. By considering the active MEA area of 20.25 cm^2 the NH_4^+ amount is estimated to be 8.0 ‰ related to the applied NH_3 amount.

This shows that ammonium is indeed incorporated into the MEA. However, the detected amount is low compared to the applied NH_3 amount, so that further effects play a role inside the HT-PEMFC. On one hand, Figure 3 showed CV clarifying the additional presence of redox active nitrogen species interacting with the catalyst and on other hand, interaction of ammonia or rather ammonium due to acidic environment with the electrolyte membrane might cause irreversible incorporation and damage, so that the membrane gets thinner as depicted in Figure 6. Also, unreacted NH_3 might leave the cell with the exhaust gas.

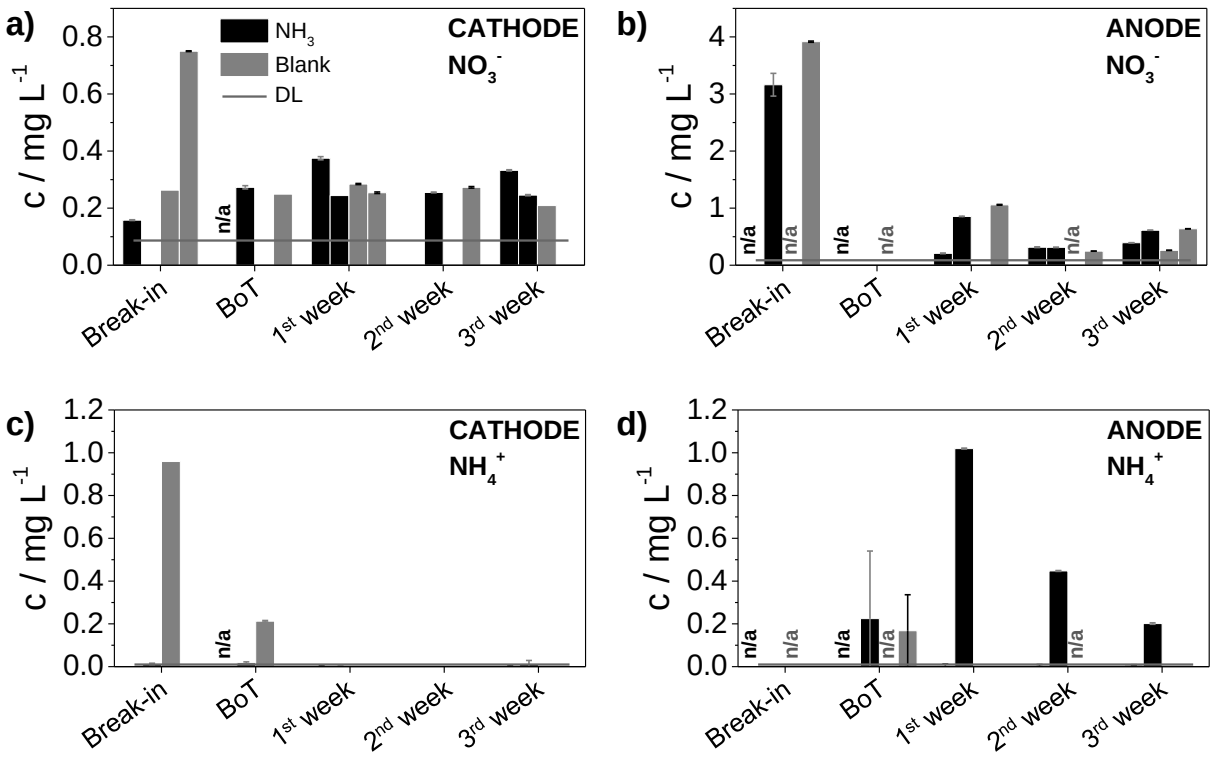

Figure 7 Concentration of (a,b) nitrate and (c,d) ammonium in cathodic and anodic waters produced during "NH_3" and "blank" operation with detection limit (DL) during IC measurement.

pH values of the water samples after third week of cell operation are listed in Table 3. The pH of these samples is most representative for comparing NH_3-contaminated cell with the non-contaminated cell, because the cell operation of 500 h was completed at this time. Slight acidic values are measured in all cases caused by occurrence of phosphoric acid electrolyte discharge, which is shown here to be independent from presence of NH_3. This supports the IC results in Figure 7c-d) that excluded higher discharge of ammonium ions which would influence the pH here to larger values. Furthermore, independency from anode or cathode site is demonstrated in Table 3, so that any dominating acid-base processes leading to discharges on anode or cathode site are excluded here as well.

Table 3 pH values of anode and cathode waters after third week of cell operation in case of NH_3-contaminated and non-contaminated cell operation.

Cell operation	Anode	Cathode
Blank	6.3	5.9
NH_3	6.2	6.0

Because the CV results in Figure 3 revealed interaction of nitrogen species stemming from NH_3 with the cathodic platinum catalyst, TEM was used to visualize the platinum particles after cell operation. Figure 8 compares TEM images and distribution of Pt particle diameters of the cathodes. Next to the catalysts of MEAs after first NH_3 and first blank operation, the catalyst of a pristine MEA from identical manufacturing batch was analyzed in same way and shows an averaged Pt particle diameter of 4.06±1.33 nm. In the following, we assume that differences in particle sizes of the tested MEAs are due to the cell operations, since all MEAs considered here are from the same manufacturing batch. Both MEAs exposed to HT-PEMFC operation consist of larger Pt particles with diameters of 4.82±1.63 nm and 4.36±1.52 nm. This is obviously traced back to the cell operation itself and exposure to a cathodic potential of approx. 0.65 V at 160 °C in acidic environment as frequently discussed in literature.[46, 54] However, after presence of NH_3 the size of Pt particles counts 4.82±1.63 nm, whereas the size after the blank operation counts

4.36±1.52 nm. That means that the MEA without exposure to NH_3 possesses only a Pt particle growth of 7 %, whereas the MEA exposed to NH_3 shows a growth of 19 %. This demonstrates that interaction of contaminating nitrogen species with the platinum catalyst strengthens its particle growth. CV experiments in Figure 3 showed a slight larger loss of ECSA in case of NH_3 presence, so that this loss is shown here to be caused by Pt particle growth. This deterioration of catalyst degradation has its origin in the platinum surface chemistry, which is obviously slightly influenced by nitrogen-containing adsorbates in this study. Several degradation paths of platinum are known. Next to detachment from or migration on the carbon support of whole particles, platinum surface atoms of the particles can dissolve followed by downstream processes of simple discharge or re-precipitation elsewhere.[46, 54] The latter process can consequence Pt particle growth based on Ostwald-Ripening[61] and is investigated by use of TEM in Figure 8. Because the thermodynamic impact factors on Pt dissolution naming electrode potential, pH and temperature[62-63] are similar in both cell operations, the reason lies in adsorption of nitrogen species on the Pt surface. Thereby, the surface energy might be increased, which directly enforces Pt dissolution and Ostwald-Ripening to reduce surface energy by the particle size effect of Gibbs-Thompson.[61, 64-65]

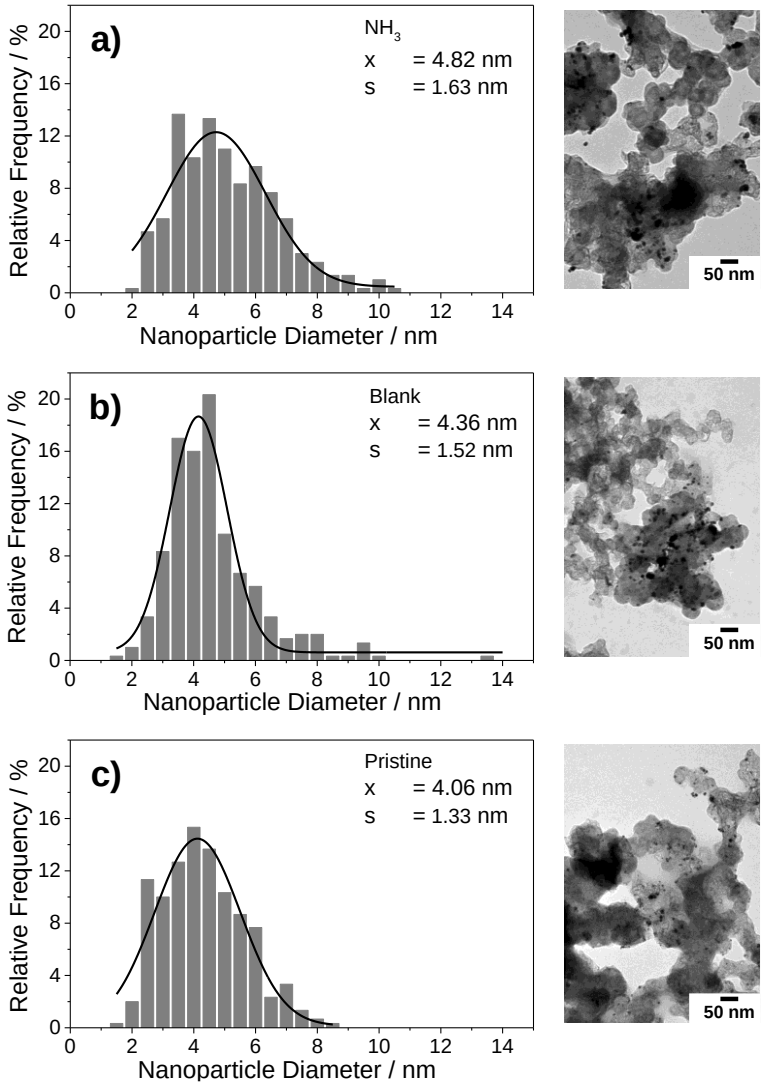

Figure 8 Platinum particle size distribution and TEM images in case of the catalysts of (a) the first "NH_3" test, (b) the first "blank" test (raw data shown in [23]) and (c) a pristine MEA of the same manufacturing charge (raw data shown in [23]).

4 Conclusions

HT-PEM fuel cells were operated for 500 h using ammonia contaminated air and analyzed on the degradation effects. The presence of ammonia caused a significant linear loss of the cell voltage, which demonstrates the high sensitivity of the HT-PEM technology to this air pollutant. Impedance spectroscopy revealed an affected proton conductivity of the electrolyte membrane, and µ-CT imaging showed undefined interfaces between membrane and catalyst layers and a significantly thinned membrane after contamination. It was verified by ion chromatography on product waters that neither acid-base reactions and discharge of NH_4^+ nor electro-oxidation and discharge of NO_3^- are predominant processes. Ammonia gas enters the cathode, but ammonium does not leave the cell in relevant amounts, which assumes proton trapping and precipitation of ammonium phosphate salts.

Cyclic voltammetry and impedance spectroscopy further revealed partially suppressed hydrogen sorption and an increased charge transfer resistance of the cathode. Electro-oxidation of ammonia can generate nitrogen species, which affected the catalyst and showed adsorption stability between 0.05–1.0 V demonstrating the difficulty of removing this species. Although the catalyst interaction with contaminating nitrogen species slightly strengthened the Pt particle growth, while the ECSA did not significantly change.

In conclusion, this study provides a better understanding of electrochemical, chemical and physical processes in HT-PEMFC degradation caused by ammonia and in particular reveals the consequences for the HT-PEM fuel cell stability. Two processes naming formation and incorporation of ammonium species inside the HT-cell as well as formation of redox active nitrogen species occur. The main reason for HT-PEMFC performance loss was found to be the deterioration of proton conductivity and electrode kinetics caused by significant electrolyte degradation through the accumulative remaining of contaminants based on NH_3 inside the HT-PEMFC.

Acknowledgements

The financial support of the Federal Ministry of Economics and Technology and the German Federation of Industrial Research Associations (AiF) with further support of the Institute of Energy and Environmental Technology e.V. (IUTA) and the Industrial Collective Research (IGF) in frame of the project HT-Kathodenluft II (reference number 19815N) is greatly appreciated. The authors further thank the Electron and Light Microscopy Service Unit of the Carl von Ossietzky University of Oldenburg for the use of the imaging facilities and Lisa Vogelsang, Tanja Zierdt and Julia Hülstede for their support in measurements. Last, the authors gratefully acknowledge the permission of C.R. Graves (DTU Energy) for use of the software *RAVDAV* to perform impedance fittings.

References

[1] R. E. Rosli, A. B. Sulong, W. R. W. Daud, M. A. Zulkifley, T. Husaini, M. I. Rosli, E. H. Majlan, M. A. Haque, *Int. J. Hydrogen Energy* **2017**, *42*, 9293-9314.

[2] S. S. Araya, F. Zhou, V. Liso, S. L. Sahlin, J. R. Vang, S. Thomas, X. Gao, C. Jeppesen, S. K. Kær, *Int. J. Hydrogen Energy* **2016**, *41*, 21310-21344.

[3] T. J. Schmidt, J. Baurmeister, *ECS Trans.* **2006**, *3*, 861-869.

[4] Umweltbundesamt, *Emissionen ausgewählter Luftschadstoffe nach Quellkategorien*, **2019**..

[5] X. Cheng, Z. Shi, N. Glass, L. Zhang, J. Zhang, D. Song, Z.-S. Liu, H. Wang, J. Shen, *J. Power Sources* **2007**, *165*, 739-756.

[6] S. Wang, J. Nan, C. Shi, Q. Fu, S. Gao, D. Wang, H. Cui, A. Saiz-Lopez, B. Zhou, *Sci. Rep.* **2015**, *5*, 15842.

[7] P. W. G. Groot Koerkamp, J. H. M. Metz, G. H. Uenk, V. R. Phillips, M. R. Holden, R. W. Sneath, J. L. Short, R. P. P. White, J. Hartung, J. Seedorf, M. Schröder, K. H. Linkert, S. Pedersen, H. Takai, J. O. Johnsen, C. M. Wathes, *Journal of Agricultural Engineering Research* **1998**, *70*, 79-95.

[8] R. Borup, E. Brosha, F. Garzon, B. Pivovar, T. Rockward, T. Springer, F. Uribe, I. Urdampilleta, J. Valerio, in *DOE Hydrogen, Fuel Cells and Infrastructure Technologies 2007 Kickoff Meeting*, **2007**.

[9] R. Mohtadi, W.-k. Lee, J. W. Van Zee, *J. Power Sources* **2004**, *138*, 216-225.

[10] A. Talke, U. Misz, G. Konrad, A. Heinzel, *J. Electrochem. Soc.* **2018**, *165*, F3111-F3117.

[11] O. A. Baturina, K. E. Swider-Lyons, *J. Electrochem. Soc.* **2009**, *156*, B1423-B1430.

[12] R. Borup, J. Meyers, B. Pivovar, Y. S. Kim, R. Mukundan, N. Garland, D. Myers, M. Wilson, F. Garzon, D. Wood, P. Zelenay, K. More, K. Stroh, T. Zawodzinski, J. Boncella, J. E. McGrath, M. Inaba, K. Miyatake, M. Hori, K. Ota, Z. Ogumi, S. Miyata, A. Nishikata, Z. Siroma, Y. Uchimoto, K. Yasuda, K.-i. Kimijima, N. Iwashita, *Chem. Rev.* **2007**, *107*, 3904-3951.

[13] Y. Nagahara, S. Sugawara, K. Shinohara, *J. Power Sources* **2008**, *182*, 422-428.

[14] J. Fu, M. Hou, C. Du, Z. Shao, B. Yi, *J. Power Sources* **2009**, *187*, 32-38.

[15] Zentrum für BrennstoffzellenTechnik ZBT GmbH, *Maßnahmen zur Erhöhung der Lebensdauer von Hochtemperatur-PEM-Brennstoffzellen unter schadstoffbelasteter Luft*, in *Innovationsreport Industrielle Gemeinschaftsforschung* **2016**.

[16] Y. Garsany, O. A. Baturina, K. E. Swider-Lyons, *J. Electrochem. Soc.* **2007**, *154*, B670-B675.

[17] Y. Garsany, O. A. Baturina, K. E. Swider-Lyons, *J. Electrochem. Soc.* **2009**, *156*, B848-B855.

[18] Y. Garsany, B. D. Gould, O. A. Baturina, K. E. Swider-Lyons, *Electrochemical and Solid-State Letters* **2009**, *12*, B138.
[19] T. Reshetenko, V. Laue, U. Krewer, K. Artyushkova, *J. Power Sources* **2019**, *438*, 226949.
[20] T. Reshetenko, V. Laue, U. Krewer, K. Artyushkova, *J. Power Sources* **2020**, *458*, 228032.
[21] C. Quijada, J. L. Vázquez, J. M. Pérez, A. Aldaz, *J. Electroanal. Chem.* **1994**, *372*, 243-250.
[22] C. Quijada, A. Rodes, J. L. Vazquez, J. M. Perez, A. Aldaz, *J. Electroanal. Chem.* **1995**, *398*, 105-115.
[23] D. Schonvogel, J. Büsselmann, P. Wagner, H. Kraus, U. Misz, H. Langnickel, A. Dyck, *Int. J. Hydrogen Energy* **2020**, *46*, 11.
[24] M. Chen, C. Du, J. Zhang, P. Wang, T. Zhu, *J. Power Sources* **2011**, *196*, 620-626.
[25] D. Schonvogel, J. Büsselmann, P. Wagner, A. Dyck, *ECS Trans.* **2020**, *98*, 267-276.
[26] X. Zhang, U. Pasaogullari, T. Molter, *Int. J. Hydrogen Energy* **2009**, *34*, 9188-9194.
[27] Zentrum für BrennstoffzellenTechnik ZBT GmbH, *Evaluierung der kathodenseitigen Schädigungsmechanismen durch partikuläre und gasförmige Luftschadstoffe mit Hilfe von elektrochemischen Messmethoden zur Standzeiterhöhrung von PEM-Brennstoffzellen (Kathodenluft II)*, in *Innovationsreport Industrielle Gemeinschaftsforschung* **2012**.
[28] R. Halseid, P. J. S. Vie, R. Tunold, *J. Power Sources* **2006**, *154*, 343-350.
[29] R. Halseid, J. S. Wainright, R. F. Savinell, R. Tunold, *J. Electrochem. Soc.* **2007**, *154*, B263-B270.
[30] Y. A. Gomez, A. Oyarce, G. Lindbergh, C. Lagergren, *J. Electrochem. Soc.* **2018**, *165*, F189-F197.
[31] X.-Z. Yuan, H. Li, Y. Yu, M. Jiang, W. Qian, S. Zhang, H. Wang, S. Wessel, T. T. H. Cheng, *Int. J. Hydrogen Energy* **2012**, *37*, 12464-12473.
[32] F. Isorna Llerena, A. de las Heras Jiménez, E. López González, F. Segura Manzano, J. M. Andújar Márquez, *Fuel Cells* **2019**, *19*, 651-662.
[33] S. T. Szymanski, G. A. Gruver, M. Katz, H. R. Kunz, *J. Electrochem. Soc.* **1980**, *127*, 1440.
[34] K.-S. Lee, J. S. Spendelow, Y.-K. Choe, C. Fujimoto, Y. S. Kim, *Nature Energy* **2016**, *1*, 16120.
[35] G. Cinti, V. Liso, S. L. Sahlin, S. S. Araya, *Energies (Open Access Journal)* **2020**, *13*, 1-17.
[36] A. Dushina, D. Schonvogel, Y. Fischer, J. Büsselmann, A. Dyck, P. Wagner, *ECS Trans.* **2020**, *98*, 537-552.
[37] H. Schmies, D. Schonvogel, J. Büsselmann, P. Wagner, A. Dyck, *ECS Trans.* **2020**, *98*, 99-107.
[38] F. J. Pinar, M. Rastedt, N. Pilinski, P. Wagner, A. Dyck, *Int. J. Hydrogen Energy* **2017**, *42*, 13860-13875.
[39] F. J. Pinar, N. Pilinski, P. Wagner, *AIChE J.* **2016**, *62*, 217-227.
[40] C. R. Graves, "RAVDAV data analysis software, version 0.9.7." **2012**.
[41] J. Büsselmann, M. Rastedt, V. Tullius, K. Yezerska, A. Dyck, P. Wagner, *Int. J. Hydrogen Energy* **2019**, *44*, 19384-19394.
[42] M. Rastedt, J. Büsselmann, V. Tullius, P. Wagner, A. Dyck, *Fuel Cells* **2018**, *18*, 113-122.
[43] S. Yu, L. Xiao, B. C. Benicewicz, *Fuel Cells* **2008**, *8*, 165-174.
[44] S. Galbiati, A. Baricci, A. Casalegno, R. Marchesi, *Int. J. Hydrogen Energy* **2013**, *38*, 6469-6480.
[45] T. Søndergaard, L. N. Cleemann, H. Becker, D. Aili, T. Steenberg, H. A. Hjuler, L. Seerup, Q. Li, J. O. Jensen, *J. Power Sources* **2017**, *342*, 570-578.
[46] Y. Shao-Horn, W. C. Sheng, S. Chen, P. J. Ferreira, E. F. Holby, D. Morgan, *Top. Catal.* **2007**, *46*, 285-305.
[47] A. Zana, J. Speder, M. Roefzaad, L. Altmann, M. Bäumer, M. Arenz, *J. Electrochem. Soc.* **2013**, *160*, F608-F615.
[48] S. Guo, S. Zhang, S. Sun, *Angew. Chem.* **2013**, *125*, 8686-8705.
[49] P. Urchaga, S. Baranton, C. Coutanceau, G. Jerkiewicz, *Langmuir* **2012**, *28*, 3658-3663.
[50] R. M. Darling, J. P. Meyers, *J. Electrochem. Soc.* **2003**, *150*, A1523-A1527.
[51] D. Schonvogel, J. Hülstede, P. Wagner, I. Kruusenberg, K. Tammeveski, A. Dyck, C. Agert, M. Wark, *J. Electrochem. Soc.* **2017**, *164*, F995-F1004.
[52] F. Zhou, S. J. Andreasen, S. K. Kær, D. Yu, *Int. J. Hydrogen Energy* **2015**, *40*, 2833-2839.
[53] J. H. Jung, H. J. Park, J. Kim, S. H. Hur, *J. Power Sources* **2014**, *248*, 1156-1162.

[54] J. Monzo, D. F. van der Vliet, A. Yanson, P. Rodriguez, *Phys. Chem. Chem. Phys.* **2016**, *18*, 22407-22415.
[55] M. Arenz, A. Zana, *Nano Energy* **2016**, *29*, 299-313.
[56] V. Bandlamudi, P. Bujlo, V. Linkov, S. Pasupathi, *Fuel Cells* **2019**, *19*, 231-243.
[57] R. Halseid, M. Heinen, Z. Jusys, R. Jürgen Behm, *J. Power Sources* **2008**, *176*, 435-443.
[58] J. Büsselmann, M. Rastedt, T. Klicpera, K. Reinwald, H. Schmies, A. Dyck, P. Wagner, *Energies* **2020**, *13*, 567.
[59] F. J. Pinar, M. Rastedt, N. Pilinski, P. Wagner, *Fuel Cells* **2015**, *15*, 140-149.
[60] R. Kuhn, J. Scholta, P. Krüger, C. Hartnig, W. Lehnert, T. Arlt, I. Manke, *J. Power Sources* **2011**, *196*, 5231-5239.
[61] W. Ostwald, *Z. Phys. Chem.* **1900**, *34*, 495–503.
[62] M. J. N. Pourbaix, *Atlas of Electrochemical Equilibria in Aqueous Solutions*, Pergamon Press Oxford, New York, U.S.A., **1966**.
[63] M. J. N. Pourbaix, J. Van Muylder, N. de Zoubov, *Platinum Met. Rev.* **1959**, *3*, 47-53.
[64] V. Komanicky, K. C. Chang, A. Menzel, N. M. Markovic, H. You, X. Wang, D. Myers, *J. Electrochem. Soc.* **2006**, *153*, B446-B451.
[65] A. V. Virkar, Y. Zhou, *J. Electrochem. Soc.* **2007**, *154*, B540-B547.